Atomic force microscopy study of thick lamellar stacks of phospholipid bilayers

Arne Schäfer, Tim Salditt, and Maikel C. Rheinstädter*
Institut für Röntgenphysik, Georg-August-Universität Göttingen, Friedrich-Hund Platz 1, 37077 Göttingen, Germany
(Received 24 July 2007; revised manuscript received 3 December 2007; published 7 February 2008)

We report an atomic force microscopy (AFM) study on thick multilamellar stacks of approximately 10 μm thickness (about 1500 stacked membranes) of 1,2-dimyristoyl-sn-glycero-3-phoshatidylcholine deposited on silicon wafers. These thick stacks could be stabilized for measurements under excess water or solution. From the force curves we determine the compressional modulus B and the rupture force F_r of the bilayers in the gel (ripple), in the fluid phase, and in the range of critical swelling close to the main transition. We observe pronounced ripples on the top layer in the $P_{\beta'}$ (ripple) phase and find an increasing ripple period Λ_r when approaching the temperature of the main phase transition into the fluid L_α phase at about 24 °C. Metastable ripples with $2\Lambda_r$ are observed. Λ_r also increases with increasing osmotic pressure, i.e., for different concentrations of polyethylene glycol.

DOI: 10.1103/PhysRevE.77.021905 PACS number(s): 87.16.D−, 68.37.Ps, 83.85.Hf

I. INTRODUCTION

There are only a few techniques that allow the study of structures on the nanometer scale with molecular spatial resolution. Scattering experiments, such as, e.g. x-ray or neutron scattering, offer this high resolution but work in reciprocal or Fourier space, and the phase problem usually inhibits a direct transformation back into real space. The investigation of particular regions in reciprocal space nevertheless gives valuable structural information. By multiplying and stacking the corresponding surfaces or interfaces, these techniques can be made surface sensitive.

Scanning probe microscopic techniques, such as atomic force microscopy (AFM) [1] and Scanning Tunneling Microscopy, on the other hand, give high resolution real space pictures but are essentially surface sensitive. The combination of the two techniques is therefore a powerful tool to gain information about bulk *and* surface structure. In this study, we used AFM to study the surface structure of the uppermost layer of thick lamellar stacks of phospholipid bilayers under excess water and solutions. As is well known, AFM can be used to monitor biological processes under physiological conditions [2] on the cellular [3] and the molecular scale [4]. In addition to topographical maps of the sample surface, the local mechanical properties of soft samples can be measured by application of very small loading forces [5–10]. By use of the Hertz model for elastic indentations [11,12], Young's modulus E can be determined.

Phospholipid membranes have been extensively studied by AFM techniques. AFM was used to reveal information on the morphology and topology of membranes, bilayers, domains [13–17], and ripple phases [18] in real time using controlled environments [19–21]. In addition, Fourier transformation was used to corroborate the periodicity of the ripple structure [21]. Single or double bilayers on solid substrates such as, e.g., silicon or glass, are usually used for these studies, with the drawback that the underlying substrate often influences or evens governs the elastic response.

Multilamellar stacks of these model membranes are often used, particularly in scattering experiments, to maximize the scattering volume and improve signal-to-noise ratio considerably. Little is known about the surface of the top layer in these stacks because the membrane stacks are often not very stable but are easily washed away under excess water, thereby making AFM investigations very difficult. But this approach has the advantage that the interaction of the probe and the underlying substrate can be neglected. Furthermore, it allows quantification of the forces needed to compress the stack, and probing of the stability of the bilayers by determining the rupture limit. This can be done at different temperatures, i.e., in the different phases of the phospholipid membranes, the ripple phase ($P_{\beta'}$) and the fluid phase L_α. This technique might therefore offer an independent approach to the elasticity parameters, in particular to the compressional modulus B, of the stacked model membranes, as we will show below.

The elastic properties of lipid membranes, in particular in multilamellar stacks, have mainly been investigated by the analysis of thermal diffuse scattering, i.e., x-ray lineshape analysis [22,23]. This work has led to a detailed understanding of the static properties of thermal fluctuations in lipid membranes and the elasticity properties governing these fluctuations. A recent experiment [24] reported an inelastic neutron scattering study where the dispersion relation of the mesoscopic fluctuation was determined by the neutron spin echo technique, which allowed a determination of elastic parameters from dynamical properties.

According to linear smectic elasticity theory [25,26] thermal fluctuations in the fluid phase of the membranes are governed by the free energy functional (Hamiltonian) [25–27]

$$H = \int_A d^2r \sum_{n=1}^{N-1} \left(\frac{1}{2}\frac{B}{d}(u_{n+1} - u_n)^2 + \frac{1}{2}\kappa(\nabla_\parallel^2 u_n)^2 \right), \qquad (1)$$

where κ denotes the bilayer bending rigidity, A the area in the xy plane, N the number of bilayers, u_n the deviation from

*Present address: Department of Physics and Astronomy, University of Missouri–Columbia, Columbia, MO 65211, U.S.A. RheinstadterM@missouri.edu

the average position (nd) of the nth bilayer, and d the lamellar spacing. B and $K=\kappa/d$ are elastic coefficients, governing the compressional and bending modes of the smectic phase, respectively. Note that the surface tension σ can usually be neglected because of the boundary conditions, i.e., infinitely large membranes, the rims of which are not clamped and small amplitude of the fluctuations. K and B always appear as coupled parameters in scattering experiments, and only the use of aligned lipid bilayers allows a separate determination of K and B [28,29]. In this work we used AFM to get direct access to the compressional modulus B of the membrane stacks.

Our AFM experiments were motivated by the inelastic neutron scattering study [24], which reported a soft mode in the dispersion relation of the long-wavelength undulation modes close to T_m. The critical q value was found to be $q_c \approx 0.015$ Å^{-1}, equivalent to a distance in real space of $\lambda_c = 2\pi/q_c \approx 420$ Å. The relaxation rate of the collective undulations dropped by more than two orders of magnitude at q_c. A possible interpretation is that the well-known softening of phospholipid bilayers due to the decrease of the bending modulus of the bilayers, κ [30], occurs on a particular length scale only, similar to the freezing of a phonon mode at elastic phase transitions in crystals. To clarify the origin of this particular length scale we investigated the same samples that have been used for the scattering experiments, namely, thick highly oriented lamellar membrane stacks on silicon wafers, in the temperature-resolved AFM experiments.

II. MATERIALS AND METHODS

A. Atomic force microscopy

A commercial AFM (Bioscope, Digital Instruments, Santa Barbara, CA) combined with an Axiomat inverted optical microscope (Zeiss) was used for this study. The optical microscope was used to position the tip above the membranes. Soft silicon nitride cantilevers (Microlever, Park Scientific, Sunnyvale, CA) with gold reflex coating on the cantilever back side and a spring constant of about 6 mN/m were used. The spring constants were estimated from their resonant frequency, which was 18 kHz. The cantilevers had tip semiangles of 35°. The wafer with the membrane probe was magnetically attached to the microscope object stage. The microscope was resting on a granite plate supported by soft rubber bands attached to the ceiling for vibration isolation. Resistors glued to the bottom of the object stage allowed us to heat the object stage and so the probe. A PT100 temperature sensor was mounted on the silicon substrate and recorded the sample temperature during the experiments. Because of the large thermal mass of the sample stage the temperature stability was as good as 0.1 °C; the absolute accuracy was better than 0.5 °C.

B. Samples

Multilamellar samples composed of stacks of several thousands of lipid bilayers separated by layers of water, resulting in a structure of smectic-A symmetry, have been prepared. 1,2-dimyristoyl-sn-glycero-3-phoshatidylcholine (DMPC) was obtained from Avanti Polar Lipids. We then prepared highly oriented membrane stacks by spreading a solution of typically 25 mg/ml lipid in trifluoroethylene/chloroform (1:1) on 2 in. silicon wafers [31]. The mosaicity of the samples, which is a measure of the alignment with respect to the surface normal of the stacked bilayers, was determined by rocking scans to a few hundreds of a degree. The samples were carefully dried and stored for several days in a refrigerator and after that in a freezer. Note that in these conditions the membranes transform into a densely packed subgel phase, which has been characterized only recently [32]. After warming to room temperature and rehydrating, the samples then abruptly irreversibly transform into the ripple or fluid phase, respectively, and show the well-known reversible sequence of gel, ripple, and fluid phase. The temperature of the main phase transition for DMPC is at 23.4 °C. In samples, that had not been stored in freezers before, the membrane film is easily washed away under excess water and no AFM investigation was possible. We argue that the lipid film is stabilized when the border areas, which are not in contact with water or solution, are still in the very stable and dry subgel phase. The effect of osmotic pressure has been studied by measuring solutions of (Millipore) water with different concentrations of polyethylene glycol (PEG) with a molecular weight of 20 000. About 2 ml of highly pure Millipore water or Millipore-PEG solution was dropped onto the sample for the measurements, covering a sample area of about $\pi(0.5\ \text{cm})^2$, and the AFM cantilever arm was immersed into the water. Figure 1 shows a photograph of the experimental setup.

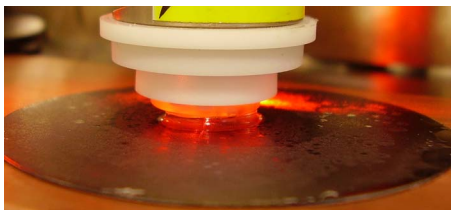

FIG. 1. (Color online) Photograph of the experimental setup. The AFM tip is completely immersed in water. The water droplet is held in place by the surface tension. Full hydration of the bilayers is guaranteed by this technique.

C. Data acquisition and analysis

Using an AFM, the surface is scanned by a nanometer-sized tip, which is mounted on an elastic cantilever arm. The size of the tip is on the order of about 40 nm. The deformation of the cantilever arm is measured and the force constant of the cantilever arms then allows determination of the force (attractive or repulsive) between sample and AFM probe. By defining a threshold, the contact point between sample and tip, and with it the height profile of the sample can be determined. A second mode of operation is to continuously scan the tip over the sample surface and continuously measure the deflection of the cantilever arm. The result is usually displayed in two-dimensional map plots.

Different scenarios for the interaction and the elastic response between tip and sample can be discussed, and are

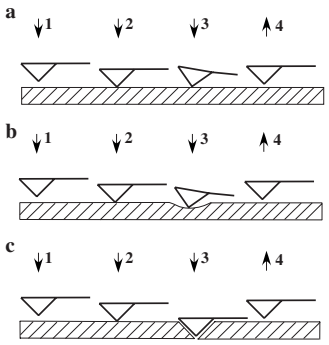

FIG. 2. Schematic of the AFM force measurement by indentation, for the case of (a) a stiff surface, (b) a soft surface, and (c) the cantilever cutting the surface. Labels 1–4 in this graph refer to the corresponding sequence in the force curves in Fig. 3: (1) The piezo is approaching the surface. (2) The AFM tip is in contact with the surface (contact point). (3) The piezo is moving down, leading to an elastic indentation in the case of a soft surface, and may cut through the surface. (4) The piezo is moving up.

exemplarily pictured in Fig. 2. When the tip approaches and comes in contact with an infinite stiff surface in Fig. 2(a) (a dry membrane stack), the cantilever arm will start to bend after being in contact. The elastic response in this case is perfectly linear and determined by the spring constant k_c of the cantilever arm. If the surface is soft or not robust (in the case of a hydrated membrane stack), the tip does indent or cut into the surface and there is little or no bending of the arm when lowering the cantilever [see Fig. 2(c)]. In general, a surface will show a mixed effect. The surface will be incised and if the force becomes too high, the tip might cut into the surface, as depicted in Fig. 2(b). In the corresponding force curves, which are shown in Figs. 3(a)–3(c) for the three cases discussed above, the deflection of the AFM cantilever is monitored as a function of its vertical position while approaching the sample. While there is a linear slope of the curve when deflected from a rigid surface in Fig. 3(a), the soft sample in Fig. 3(b) is incised when lowering the AFM tip. In Fig. 3(c), the tip is first deflected (points 1–3) but then cuts through the surface as indicated by the horizontal plateau. From the slope of these curves, normalized to an infinite stiff surface, the forces to press and cut through the membranes can be quantified [7].

D. Geometry

The elastic parameters of the bilayers which are actually probed by the AFM depend on the particular experimental geometry. The elasticity of lipid membranes spanned over small nanometer-sized pores, where the tip size is in the order of the size of the membrane with correspondingly large indentations, has been probed by AFM very recently [33]. The theoretical framework that describes the indentation of the pore-spanning bilayers has been developed and published in parallel [34] and the indentation profile of a parabolic tip and the bilayer has been carefully investigated. Note that this setup leads to strong curvature and nonlinear equations. For pore spanning membranes on large holes (tip size and indentations small as compared to the size of the membrane) the

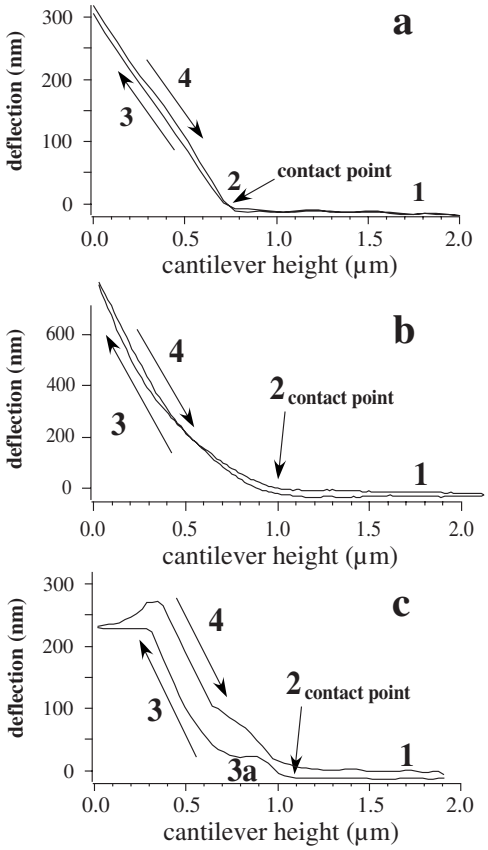

FIG. 3. (a) Typical force curve on a dry, hard membrane stack. The cantilever height is defined as the z direction. The arrows mark the contact points where the cantilever first comes in contact with the sample surface. The approach and the retraction curves are also indicated by arrows. The elastic response is linear and determined by the spring constant k_c of the cantilever (the slope of the curve). (b) Typical force curve on a soft, hydrated membrane stack. The slope of this curve is considerably smaller than that of the stiff sample. The difference results from the larger indentation of the cantilever in the softer sample. (c) In this case, after indenting the surface, the cantilever cuts through several layers when the force exceeds a characteristic threshold marked by the plateau at small cantilever heights [compare Fig. 2(c)]. The cantilever has no "resistance" and so no deflection can be measured.

assumption of small displacements is reasonable and the Young's modulus E of the membranes is probed. AFM investigations on single supported membranes allow the study of breakthrough forces, breakthrough distances, adhesion, stiffness, and topography [35,36] with a high spatial resolution.

The present work deals with very thick multilamellar stacks of solid supported membranes. Applying force onto membrane stacks is an entirely different situation from the case addressed above on single membranes. The pressure applied by the tip will lead to a local compression of the membrane stack, leading to a decrease of the interbilayer spacing d (lamellar repeat distance) from the equilibrium one. Note also that, in contrast to a uniform linear force response, some force curves exhibit horizontal plateaus, i.e., the tip lowers without deflection, indicative for a cut through the bilayers. In the linear regime, a compression of the stack

will result, over some lateral interaction area A. Apart from experimental parameters like tip radius, A will be determined by the interplay of B and K as well as the swelling state d. According to Eq. (1), a local force will lead to a compression over some interaction area A, to minimize bending and compressional energy. If for an idealized patch of area A we treat the membrane compression, in an oversimplistic approach, as a compression of flat and stiff planes, the compressional modulus B of the membrane stack can be written as the derivative of the applied force with respect to the cantilever height, normalized to the lamellar spacing d of the bilayers

$$B = \frac{d}{A}\frac{\partial F}{\partial z}. \tag{2}$$

The entire physics of smectic elasticity is now contained in the effective parameter A. The higher the bending rigidity and the lower the compressional modulus, the larger A. The basic length scale of this interplay is the smectic length scale $\lambda_c = \sqrt{K/B}$. We thus postulate that $A \propto \lambda_c^2 = K/B$, with λ_c typically on the same order of magnitude, but somewhat smaller than the interlamellar spacing d.

The approach is justified *a posteriori* by the values that are obtained for B, if typical values for λ_c are taken to estimate A. The values for B then agree well with values reported in the literature by other techniques (see below). Note, however, that it is the bending modulus $K = d\partial F/\partial z$ which determines the slope of the force curve, since B cancels out in Eq. (2).

In the following, we will however deliberately set $A = d^2$. This way the analysis of the force curve will not rely on literature values of λ_c, and the resulting effective modulus derived from the indentation experiments will be denoted as B_{ind}.

III. RESULTS AND DISCUSSION

A. Force curves

Force curves have been measured at different temperatures. The sample has been checked by deflection scans and an area clean of obvious defects like steps, holes, or kinks has been selected. Typical deflection curves as a function of cantilever height are shown in Fig. 4(a). The dry bilayer stack at 19 °C has been measured as a reference. It shows the characteristics of a rigid sample with a well-defined contact point and well-defined linear slope, as discussed in Figs. 2 and 3. After applying excess water, the response changes and the surface becomes softer with a less well-defined contact, but still linear elastic response. The situation is then completely different in the fluid phase at, e.g., $T = 26.7$ °C. When approaching, the tip is first deflected, but then cuts through the first layers, as indicated by the horizontal plateau, before it is deflected again. There is a critical deflection above which the tip is just cutting through the bilayers. Although the positions of the plateaus might slightly vary in different experiments, we found this to be a typical response in the fluid phase.

Close to the phase transition, at $T = 23.4$ °C, in the range of the critical swelling of the phospholipid bilayers, the membranes are more stable, there is no rupture of the bilayers, but initially there is only slight deflection when the tip is lowered, indicating that the stack is very soft and can easily be compressed. The slope of the curve becomes steeper at higher indentations only. From these data, B_{ind} and the rupture force F_r can be determined.

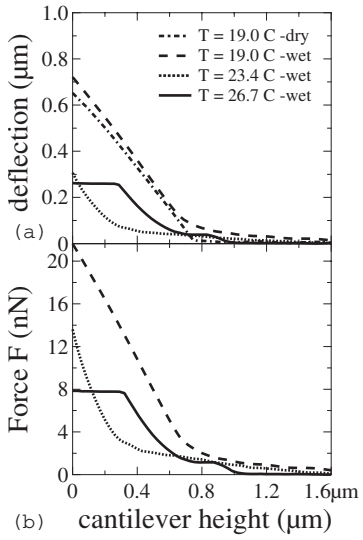

FIG. 4. (a) Force curves at different temperatures and for a dry sample. (b) Taking the dry sample as a reference, the corresponding force can be quantified.

Taking the dry sample as an ideal stiff reference, we can quantify the corresponding interaction forces. The difference from using, e.g., the silicon substrate as stiff reference is that the dry membrane could be measured *in situ*, thereby preserving the interaction between tip and sample and also the geometrical setup. Note that the normalization to the dried membrane stack cancels out all elasticity already present without excess water at ambient conditions (room temperature and humidity). The force is then calculated as $F = k_c(z - z_{\mathrm{ref}})$, where k_c is the cantilever spring constant and $(z - z_{\mathrm{ref}})$ the difference of cantilever height with respect to the (hard) reference sample. Figure 4(b) plots the resulting forces in nano-Newtons versus the cantilever height z for the different temperatures.

B has been determined from the slope of the force curves in Fig. 4(b) following Eq. (2), and is plotted in Fig. 5 for $T = 19.0$, 23.4, and 26.7 °C, i.e., in the gel (ripple) phase of the bilayers, close to the phase transition, and in the fluid phase. The corresponding lamellar spacings d cannot, of course, be determined by AFM but have additionally been measured by x-ray diffraction on multilamellar DMPC vesicles in excess water. Vesicles were prepared and used to ensure full hydration of the bilayers because the hydration can be expected to be a crucial parameter for the compressibility of the membrane stacks. While the elastic response of the membrane stack is linear in the gel phase, as indicated by the constant value for B_{ind} in Fig. 5 at $T = 19.0$ °C, elastic responses in the range of critical swelling and in the fluid phase are highly nonlinear. Table I lists values for the rupture force F_r and B, as determined from Figs. 4 and 5. In the nonlinear regimes, the values for B_{ind} and F_r are the maxima

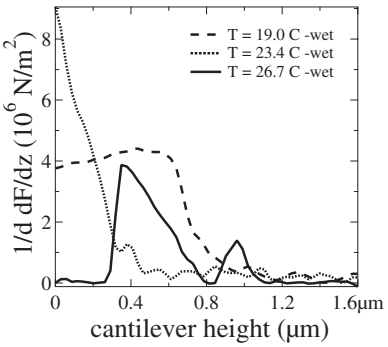

FIG. 5. Modulus B determined as $B \approx (1/d)\partial F/\partial z$ [Eq. (2)] for $T=19.0$, 23.4, and 26.7 °C, i.e., in the gel (ripple) phase of the bilayers, close to the phase transition, and in the fluid phase. While the elastic response of the membrane stack is linear in the gel phase as indicated by the constant value for $(1/d)\partial F/\partial z$ at $T=19.0$ °C, elastic responses in the range of critical swelling and in the fluid phase are highly nonlinear. Table I lists values for the rupture force F_r and B_{ind}.

and minima, respectively, of all the values that we measured.

In the gel phase, we find B_{ind} values of 4.4×10^6 N/m^2. Close to T_m, the compressional modulus more than doubles to $B_{ind}>8.3\times10^6$ N/m^2. Although the corresponding curve in Fig. 4(b) looks indeed much *softer* than in the gel phase, the slope at higher indentations is actually much steeper. The slope of the force-distance curve in the fluid phase is again smaller than in the gel phase, and B_{ind} is determined to $B>3.3\times10^6$ N/m^2 (interrupted by the bilayer rupture). All values for B agree quite well with and lie in the middle of the broad range of values reported in the literature [23,30,37,38]. While the energy to compress the membrane stack is comparable in the gel (ripple) and fluid phases, the stack is distinctly harder to compress in the range of *critical swelling*. We thus argue that AFM offers an independent determination of the compressional modulus of membrane stacks. While in scattering experiments it is usually very difficult to determine the bending modulus K and B independently from each other, the determination of force curves by AFM gives direct access to B_{ind}. Although our approach might be oversimplified, it nevertheless gives very reasonable values for the compressional modulus of the membrane stacks. The dynamic experiment in [24] gave a larger $B=1.08\times10^7$ N/m^2 in the fluid phase at 30 °C, which might be related to only partial hydration of the membranes in the neutron experiment. The bilayers were hydrated from the vapor phase and swollen to $d=54$ Å only.

TABLE I. Values for the rupture force F_r and the compressional modulus $B_{ind}\approx(1/d)(\partial F/\partial z)$ of the membrane stacks, as determined from Figs. 4 and 5. The lamellar spacing d has been determined independently by supplementary x-ray diffraction experiments on multilamellar DMPC vesicles.

T (°C)	d (Å)	F_r (nN)	$(1/d)(\partial F/\partial z)$ (10^6 N/m^2)
19.0	65.5	>20	4.4
23.4	66	>13	>8.3
26.7	63	<8	>3.9

B. Ripples on DMPC

The preparation of thick membrane stacks also allowed us to study the structure of the top bilayer and to determine the ripple periodicity Λ_r. Starting at a temperature of 18 °C, the sample was slowly heated with a rate of 0.1 °C/min, and the deflection was continuously scanned over an area of 1×1 μm^2. Static ripple patterns have been observed. To determine the corresponding ripple period Λ_r, we have selected an area of 300×300 nm^2 and Fourier transformed. From the sharp spots, the corresponding $\vec{k}$ vector and $\Lambda_r=1/|\vec{k}|$ were determined. The resulting plots are shown in Fig. 6. Figure 7 gives the resulting period for all measured temperatures. Note that there is a certain spread in the determination of Λ_r. The Fourier transform integrates over an area of 300×300 nm^2 and the occurrence of different ripple domains, i.e., different directions of the normal vectors, and static defects might lead to slightly different $|\vec{k}|$ values and periods.

From the temperature dependence of Λ_r in Fig. 7, the ripple period is initially almost constant, with values of about 100 Å in the ripple phase at temperatures $T<T_m$. Λ_r increases when approaching the main transition at about 24 °C. At temperatures in the range of T_m we find a coexistence of ripples with Λ_r and $2\Lambda_r$ (about 420 Å), visible as two diffraction spots in the Fourier transformation in Fig. 6. Figure 7 suggests a diverging ripple period when approaching T_m. Weak ripples stay visible in the Fourier spectra up to about $T=25$ °C, 1 °C above T_m. At higher temperatures in the fluid phase, no ripples can be detected.

Metastable $2\Lambda_r$ and even $4\Lambda_r$ ripples were reported earlier from AFM experiments on double bilayers [19,39] and x-ray diffraction [40]. The length scale of the metastable $2\Lambda_r$ ripples agrees quite well with the length scale of the soft mode found in a dynamical neutron study with $2\Lambda_r\approx2\pi/q_c$. We speculate that the softening in the range of the phase transition might be coupled to the occurrence of these metastable $2\Lambda_r$ ripples. A possible explanation is that bending of the bilayers might occur mainly in the interfaces between two metastable ripples. The bending modulus might thus be distinctly softer because the structure and interactions are likely to be much less well defined in the interface, and not much energy is needed to slightly change the tilt angle between the ripple flanks. From our experiments we cannot determine the structure of the super-ripple structure, i.e., whether possibly a pattern of coexisting gel and fluid domains develops within the super-ripple structure, as suggested by Heimburg [41]. It is well known that large fluid and gel domains with micrometer size coexist in the range of the main transition, which can, for instance, be observed by fluorescence microscopy techniques. The inelastic neutron scattering study in [24] and our AFM study now point to coexisting *nanodomains* with sizes of less than 50 nm, which might play a crucial role in the understanding of phospholipid bilayer dynamics and criticality in the range of T_m, the range of critical swelling [42–44]. Interestingly, the existence of coexisting gel and fluid nanodomains close to T_m

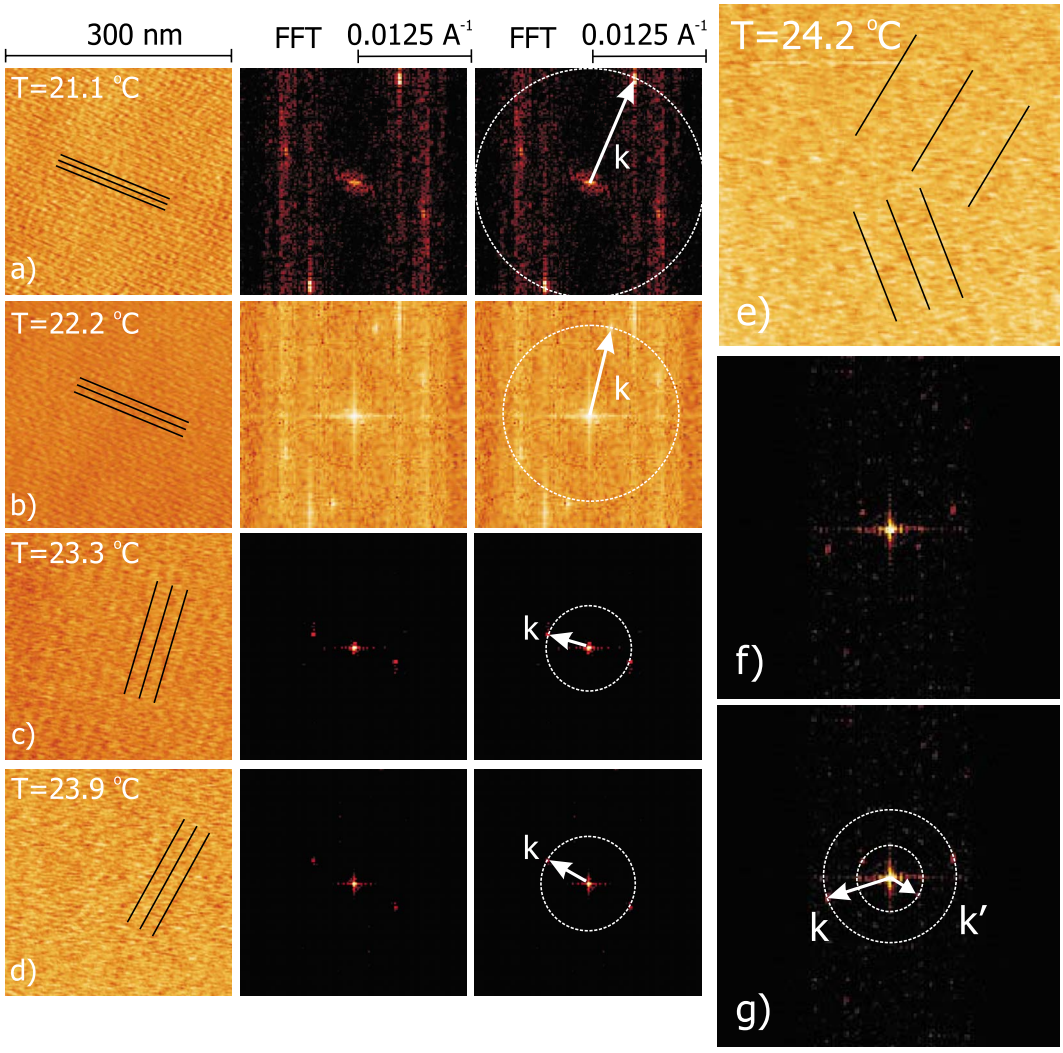

FIG. 6. (Color online) AFM deflection scans over areas of 300×300 nm^2 and the corresponding Fourier transform for selected temperatures (a) 21.1, (b) 22.2, (c) 23.3, (d) 23.9, and (e)–(g) 24.2 °C. The arrows mark the positions of diffraction spots in the Fourier spectra. The corresponding period in real space is indicated by the lines in the deflection plots. The ripple period Λ_r increases on approaching T_m (k decreases) and at the same time the ripples can be less well resolved, most likely due to a decreasing ripple amplitude. (e)–(g) Metastable $2\Lambda_r$ ripples (denoted $\mathbf{k}'$) appear at the transition temperature, which coexist with the Λ_r ripples ($\mathbf{k}$). Ripple amplitude is very small at T_m so that a Fourier transformation is needed to unambiguously determine Λ_r.

has been argued in a previous inelastic neutron scattering study [45] that investigated the collective short-wavelength dynamics in DMPC bilayers, from the coexistence of gel- and fluidlike excitations in the range of the critical swelling. The existence of coexisting small gel and fluid domains has also been argued from previous AFM investigations [20,46] to compensate the large stress which occurs at T_m due to the volume difference of the two phases. Note that [39] also reported metastable $2\Lambda_r$ ripples which were distinctly "softer" than the Λ_r ripples.

C. Ripple period on DMPC and PEG

PEG exerts an osmotic pressure on the membrane stack, which results in a slightly reduced lamellar spacing d, as is observed when lowering the hydration of the stacked membranes. We have prepared solutions of 5.8%, 12.1%, and

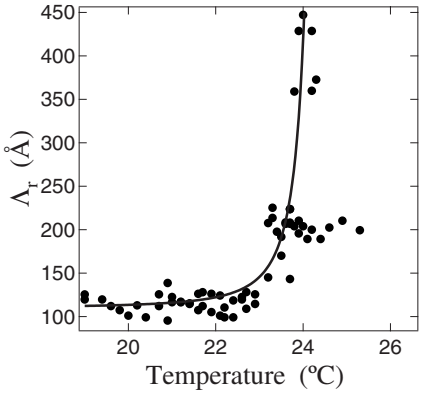

FIG. 7. Temperature dependence of the ripple period Λ_r as determined from the spots (Bragg reflections) in the Fourier transforms in Fig. 6. Λ_r increases on approaching the main transition at about 24 °C. At temperatures close to T_m there is a coexistence of ripples with Λ_r and $2\Lambda_r$. Solid line is a guide to the eye.

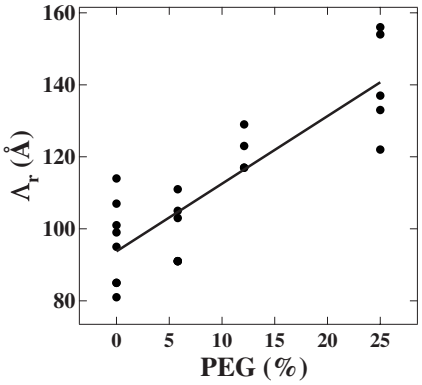

FIG. 8. Ripple period Λ_r for different concentrations of PEG, i.e., for different osmotic pressures. Solid line is a linear fit. Several measurements have been made at each concentration. The error bars are reasonably defined by the scattering of the Λ_r, values which arise from integrating over several ripple domains in the AFM measurements in Fig. 6. The average Λ_r values increase with increasing osmotic pressure from about 100 to 140 Å.

25% PEG in Millipore water. About 2 ml of the solution was then dropped onto the sample and the AFM head immersed. All scans were taken at $T=19$ °C, in the ripple phase of the DMPC bilayers, where ripples could easily be observed. For each concentration, several scans were taken. The resulting data are shown in Fig. 8. Error bars might be defined by the spread in Λ_r in the different scans for the same concentration. Although the error bars are relatively large, there is a clear tendency: the ripple period Λ_r increases from about 100 Å for DMPC under pure water to about 140 Å for DMPC in 25% PEG. Table II lists values for PEG concentration, corresponding osmotic pressure, and d spacings of the stacked membranes that cannot be accessed by AFM but were taken from the supplementary x-ray diffraction experiments. Using values from Chu *et al.* [30], the effect of an increasing PEG concentration can be compared to lowering the hydration. The corresponding values for RH are also given in Table II.

The osmotic pressure exerted by the polymer leads to an increase of the ripple period Λ_r while the lamellar spacing d decreases. A correlation between ripple period and thickness of the water layer, i.e., hydration, was established almost 20 years ago [48] by x-ray diffraction of vesicles. Although the technique was basically bulk sensitive and the samples vesicles instead of highly oriented solid supported bilayers, the authors found an increasing Λ_r with decreasing lamellar spacing d. According to an AFM study [39], the occurrence of ripples is a consequence of interbilayer interaction and no ripples are observed on single bilayers. The increasing ripple period most likely stems from an increasing interaction between the bilayers when decreasing the bilayer distance. The ripples might, for instance, "round out," i.e., the amplitude and the tilt angle decrease, leading to an increased period. But a structural investigation using x-ray or neutron diffraction is clearly needed to determine the temperature-dependent ripple structure before drawing further conclusions.

TABLE II. Osmotic pressure P for the different PEG concentrations and corresponding d-spacing [23,44,47]. Values for the relative humidity (RH) can be taken from, e.g., Fig. 3 in [30]. Λ_r periods have been taken as the average values determined from Fig. 8.

% PEG	P (dyn/cm^2)	P (10^5 Pa)	d (Å^{-1})	RH (%)	Λ_r (Å)
0	0	0	65.5	100	100
5.8	5.55	0.35	60	99.98	105
12.1	6.08	1.2	58	99.925	120
25	6.94	8.7	54	99.525	140

IV. CONCLUSION

In conclusion we present an AFM study of highly aligned, solid supported thick lamellar stack of phospholipid bilayers under excess water and water-PEG solutions. Our investigation proves the feasibility of working with AFM and thick samples in excess water. These samples are often used to study structural and dynamic properties of model membrane systems in x-ray and neutron scattering experiments. An advantage as compared to single or double bilayers is that in thick samples the interaction between the AFM tip and the substrate can be neglected. From force curves at different temperatures, we determined values for the compressional modulus B and the rupture force F_r of the membrane stacks in the ripple and the fluid L_α phase and in the regime of critical swelling. The values for B_{ind} are in good agreement with the literature values for B and this approach allows us to determine B independently of other elasticity parameters.

The uppermost layer shows pronounced ripples in the $P_{\beta'}$ phase. We find an increasing ripple periodicity Λ_r when approaching the temperature of the main transition at $T_m=24$ °C. Close to T_m we observe coexisting metastable ripples with $2\Lambda_r \approx 420$ Å. The length scale of these ripples agrees well with the length scale of a soft mode in the dispersion relation of the long-wavelength undulation modes reported in a recent inelastic neutron scattering study and might be responsible for the well-known softening of phospholipid bilayers in the range of the critical swelling. The ripple period Λ_r increases also with increasing osmotic pressure, most likely due to an increasing interaction between the bilayers in the stack.

ACKNOWLEDGMENTS

We acknowledge financial support from the DFG through Project No. SA 772/8-2. M.C.R. would like to thank the Institut für Röntgenphysik, Göttingen, Germany, for many kind hospitality during his very enjoyable sabbatical leave. We would like to thank E. Kats for critically commenting on the manuscript in its final version.

[1] G. Binnig, C. F. Quate, and Ch. Gerber, Phys. Rev. Lett. **56**, 930 (1986).
[2] B. Drake, C. Prater, A. Weisenhorn, S. Gould, T. Albrecht, C. Quate, D. Cannell, H. Hansma, and P. Hansma, Science **243**, 1586 (1989).
[3] M. Fritz, M. Radmacher, and H. Gaub, Biophys. J. **66**, 1328 (1994).
[4] M. Radmacher, M. Fritz, H. Hansma, and P. Hansma, Science **265**, 1577 (1994).
[5] N. Tao, S. Lindsay, and S. Lees, Biophys. J. **63**, 1165 (1992).
[6] M. Radmacher, M. Fritz, and P. Hansma, Biophys. J. **69**, 264 (1995).
[7] A. Schäfer and M. Radmacher, Acta Biomater. **1**, 273 (2005).
[8] A. Weisenhorn, M. Khorsandi, S. Kasas, V. Gotozos, M. Celio, and H. Butt, Acta Biomater. **4**, 106 (1993).
[9] C. Rotsch, K. Jacobson, and M. Radmacher, Proc. Natl. Acad. Sci. U.S.A. **96**, 921 (1999).
[10] M. Radmacher, M. Fritz, M. Kacher, J. Cleveland, and P. Hansma, Biophys. J. **70**, 556 (1996).
[11] H. Hertz, J. Reine Angew. Math. **92**, 156 (1881).
[12] I. Sneddon, Int. J. Eng. Sci. **3**, 47 (1965).
[13] L. Perino-Gallice, G. Fragneto, U. Mennicke, T. Salditt, and F. Rieutord, Eur. Phys. J. E **8**, 275 (2002).
[14] M.-C. Giocondi, L. Pacheco, P. E. Milhiet, and C. le Grimellec, Ultramicroscopy **86**, 151 (2000).
[15] Y. Dufrene and G. Lee, Biochim. Biophys. Acta **1509**, 14 (2000).
[16] H.-A. Kolb, O. Enders, and R. Schauer, Appl. Phys. A: Mater. Sci. Process. **68**, 247 (1999).
[17] M. Beckmann, P. Nollert, and H.-A. Kolb, J. Membr. Biol. **161**, 227 (1998).
[18] C. Leidy, T. Kaasgaard, J. Croew, O. Mouritsen, and K. Jorgensen, Biophys. J. **83**, 2625 (2002).
[19] T. Kaasgaard, C. Leidy, J. Croew, O. Mouritsen, and K. Jorgensen, Biophys. J. **85**, 350 (2003).
[20] F. Tokumasu, A. Jin, and A. Dvorak, J. Electron Microsc. **51**, 1 (2002).
[21] O. Enders, A. Ngezahayo, M. Wiechmann, F. Leisen, and H.-A. Kolb, Biophys. J. **87**, 2522 (2004).
[22] C. R. Safinya, D. Roux, G. S. Smith, S. K. Sinha, P. Dimon, N. A. Clark, and A. M. Bellocq, Phys. Rev. Lett. **57**, 2718 (1986).
[23] H. I. Petrache, N. Gouliaev, S. Tristram-Nagle, R. Zhang, R. M. Suter, and J. F. Nagle, Phys. Rev. E **57**, 7014 (1998).
[24] M. C. Rheinstädter, W. Häußler, and T. Salditt, Phys. Rev. Lett. **97**, 048103 (2006).
[25] A. Caillé, C. R. Seances Acad. Sci., Ser. B **274**, 891 (1972).
[26] N. Lei, C. Safinya, and R. Bruinsma, J. Phys. II **5**, 1155 (1995).
[27] N. Lei, Ph.D. Dissertation, Rutgers University, 1993.
[28] Y. Lyatskaya, Y. Liu, S. Tristram-Nagle, J. Katsaras, and J. F. Nagle, Phys. Rev. E **63**, 011907 (2000).
[29] T. Salditt, M. Vogel, and W. Fenzl, Phys. Rev. Lett. **90**, 178101 (2003).
[30] N. Chu, N. Kučerka, Y. Liu, S. Tristram-Nagle, and J. F. Nagle, Phys. Rev. E **71**, 041904 (2005).
[31] C. Münster, T. Salditt, M. Vogel, R. Siebrecht, and J. Peisl, Europhys. Lett. **46**, 486 (1999).
[32] H. W. Meyer, K. Semmler, W. Rettig, W. Pohle, A. S. Ulrich, S. Grage, C. Selle, and P. J. Quinn, Chem. Phys. Lipids **105**, 149 (2000).
[33] S. Steltenkamp, M. M. Müller, M. Deserno, C. Hennesthal, C. Steinem, and A. Janshoff, Biophys. J. **91**, 217 (2006).
[34] D. Norouzi, M. M. Müller, and M. Deserno, Phys. Rev. E **74**, 061914 (2006).
[35] S. Künnecke, D. Krüger, and A. Janshoff, Biophys. J. **86**, 1545 (2004).
[36] S. Künnecke, D. Krüger, and A. Janshoff, ChemPhysChem **5**, 989 (2004).
[37] Y. Liu and J. F. Nagle, Phys. Rev. E **69**, 040901(R) (2004).
[38] G. Pabst, J. Katsaras, V. A. Raghunathan, and M. Rappolt, Langmuir **19**, 1716 (2003).
[39] Y. Fang and J. Yang, J. Phys. Chem. **100**, 15614 (1996).
[40] J. Katsaras, S. Tristram-Nagle, Y. Liu, R. L. Headrick, E. Fontes, P. C. Mason, and J. F. Nagle, Phys. Rev. E **61**, 5668 (2000).
[41] T. Heimburg, Biophys. J. **78**, 1154 (2000).
[42] F. Y. Chen, W. C. Hung, and H. W. Huang, Phys. Rev. Lett. **79**, 4026 (1997).
[43] J. Nagle, H. Petrache, N. Gouliaev, S. Tristram-Nagle, Y. Liu, R. Suter, and K. Gawrisch, Phys. Rev. E **58**, 7769 (1998).
[44] P. C. Mason, J. F. Nagle, R. M. Epand, and J. Katsaras, Phys. Rev. E **63**, 030902(R) (2001).
[45] M. C. Rheinstädter, C. Ollinger, G. Fragneto, F. Demmel, and T. Salditt, Phys. Rev. Lett. **93**, 108107 (2004).
[46] A. F. Xie, R. Yamada, A. A. Gewirth, and S. Granick, Phys. Rev. Lett. **89**, 246103 (2002).
[47] U. Mennicke, D. Constantin, and T. Salditt, Eur. Phys. J. E **20**, 221 (2006).
[48] D. C. Wack and W. W. Webb, Phys. Rev. Lett. **61**, 1210 (1988).